JACS
JOURNAL OF THE AMERICAN CHEMICAL SOCIETY

Article

pubs.acs.org/JACS

Electron Transfer Facilitated by Dendrimer-Encapsulated Pt Nanoparticles Across Ultrathin, Insulating Oxide Films

Nevena Ostojic, James H. Thorpe, and Richard M. Crooks*

Department of Chemistry, Center for Electrochemistry, and the Center for Nano- and Molecular Science and Technology, The University of Texas at Austin, 105 E. 24th Street, Stop A5300, Austin, Texas 78712-1224, United States

Supporting Information

ABSTRACT: Electrocatalytic oxygen reduction at carbon electrodes fully passivated by Al_2O_3 is reported. Specifically, pyrolyzed polymer film (PPF) electrodes were prepared and then coated with pinhole-free Al_2O_3 layers ranging in thickness from 2.5 to 5.7 nm. All of these ultrathin oxide film thicknesses completely passivated the PPF electrodes, resulting in no faradaic current for either inner-sphere or outer-sphere electrochemical reactions. The electrodes could, however, be reactivated by immobilizing Pt dendrimer-encapsulated nanoparticles (DENs), containing an average of 55 atoms each, on the oxide surface. These PPF/Al_2O_3/Pt DEN electrodes were completely stable under a variety of electrochemical and solution conditions, and they are active for simple electron-transfer reactions and for more complex electrocatalytic processes. This approach for preparing well-defined oxide electrodes opens the door to a better understanding of the effect of oxide supports on reactions electrocatalyzed by metal nanoparticles.

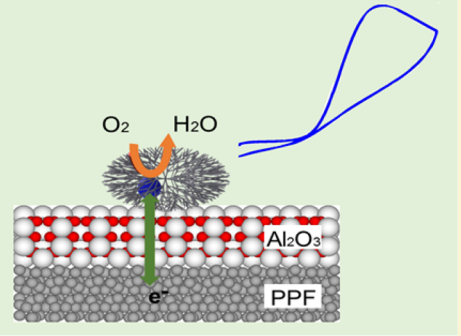

INTRODUCTION

In this paper we report that fully passivating, ultrathin (2.5 nm-thick) Al_2O_3 layers can be deposited onto carbon electrodes via atomic layer deposition (ALD). More importantly, however, subsequent adsorption of Pt dendrimer-encapsulated nanoparticles (DENs)[1−4] onto the oxide surface leads to an electrocatalytically active interface (Scheme 1). These results are important, because they provide a general approach for studying electrocatalytic reactions on nonconductive oxide surfaces.

The dendrimer-templating method was first introduced by our group in 1998,[5] and since then it has been extensively used for synthesizing a broad range of nanoparticles (NPs).[2,3,5,6] DENs are prepared by combining dendrimers and metal ions in fixed stoichiometric ratios, and then adding a reducing reagent to convert the metal ions to atoms. The atoms agglomerate within the dendrimer leading to particles in the size range of ~0.5−2.2 nm. This is the important size range over which the catalytic properties of metals change quickly and in interesting ways.[7,8] Indeed, DENs are especially useful for understanding electrocatalytic reactions because they are well-defined in size, structure, and composition, and this in turn provides a means to establish structure−function relationships.[1,2,9−13] For the present study, the dendrimer host also provides important functions: stabilizing the DENs against aggregation and immobilizing them on the electrode surface via specific interactions with the oxide.

Although structurally not as well-defined as DENs, metal oxides deposited via ALD are the best option available for our planned electrocatalysis studies. Because it is electrically

Scheme 1

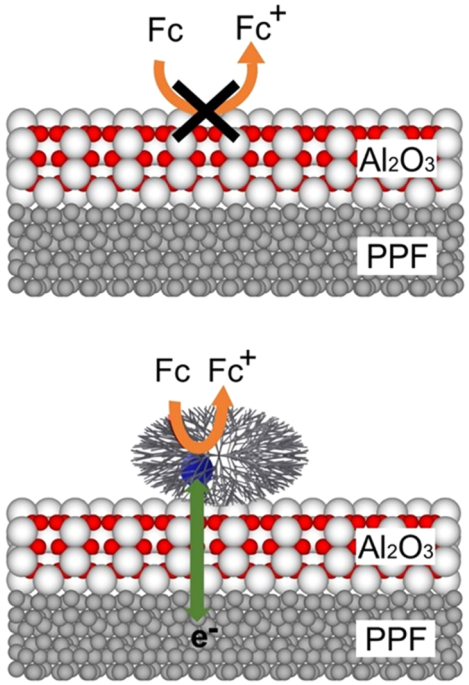

Received: March 26, 2016
Published: May 18, 2016

DOI: 10.1021/jacs.6b03149
J. Am. Chem. Soc. 2016, 138, 6829−6837

insulating and has a low dielectric constant, we[14] and others[15−17] have used Al_2O_3 for the purposes of hindering charge-transfer between an electrode and redox molecules in solution.[14] For example, we reported that Al_2O_3 films thicker than ∼3.5 nm fully passivate electron transfer (eT) between underlying pyrolyzed polymer film (PPF) electrodes[18,19] and solution-phase ferrocenemethanol (FcMeOH).[14] Subsequently, Rose and co-workers reported that ALD-deposited Al_2O_3 films ∼5 nm thick can electrochemically passivate an underlying Si(111) electrode.[15]

The other important precedents for our findings relate to NP-mediated eT across insulating layers. Although first reported by Natan and co-workers[20,21] and then more thoroughly studied by Schiffrin and co-workers,[22−24] the interest in NP-mediated eT across ultrathin organic insulating layers picked up momentum in 2008 and 2009 when Fermin[25−29] and Gooding[30,31] independently reported that this type of eT is independent of insulating film thickness.[32] In these early publications, both groups used adsorbed AuNPs to switch on faradaic eT reactions following passivation of an electrode with self-assembled monolayers.[33] Over the past several years these results have been reproduced using different types of NPs (e.g., metals,[15,34−37] graphene,[38,39] nanotubes,[40−42] and quantum dots[26,43]) and electrodes (e.g., Au,[26,28−30] Pt,[24] carbon,[31] TiO_2,[34] and Si).[32]

The foregoing experimental observations raised questions about the underlying cause of this emergent phenomenon, and in 2010, Chazalviel and Allongue developed a theoretical model that described the principles of NP-mediated eT. They proposed that the potential across an electrode modified with an insulating layer decreases exponentially as a function of the insulating layer thickness.[44] Once NPs are deposited atop ultrathin insulating layers, however, the applied potential develops primarily at the interface between the metal NPs and electrolyte.[15,26,34,44,45] As a result, distance-independent eT recovery is observed as long as the exchange current density across the insulating layer in the metal/insulator/metal NP system is much higher than the current density at a metal/insulating layer system.[26,28,44] This means that charging of NPs by a redox molecule, rather than eT between an electrode and NPs, is the rate limiting step in such processes.[44]

Our principle interest in this type of system is in understanding how reactions electrocatalyzed by metal NPs are affected by the presence of oxide surfaces. Due to the insulating nature of most oxides, there have only been a few reports of electrocatalysis on these types of surfaces. For example, Swider-Lyons and co-workers showed that PtNPs supported on metal oxides or metal phosphates lead to enhanced electrocatalytic activity for the ORR.[46,47] Although the mechanism of this reaction is unknown, the authors hypothesized that oxides can affect the electronic states of the Pt which in turn can lead to preferential adsorption of OH on the oxide (relative to the Pt surface).[47] Similarly, Ramaker and co-workers reported that if PtNPs are supported on tantalum oxide or tantalum oxyphosphate on Vulcan carbon, the presence of phosphates and oxides can lead to a higher proton conduction to PtNPs. This in turn results in improved electrocatalytic activity of Pt for the ORR.[48]

Interestingly, increased electroactivity can also be achieved by inverting metal/insulator/metal structures. For example, Adzic and co-workers reported that deposition of SnO_2 NPs onto polycrystalline Pt electrodes (SnO_2/pc-Pt) resulted in up to a 40-fold enhancement in current for the methanol oxidation reaction (MOR) compared to naked Pt electrodes.[49] Additionally, the MOR activity was found to be strongly dependent on the number of available SnO_2/Pt contact sites and to decrease as the size of the SnO_2 NPs increased. They interpreted these results in terms of a cocatalytic mechanism in which the reaction occurs at the contact line between Pt and the SnO_2 NPs. Moreover, the relationship between NP size and activity was thought to be a consequence of the formation of reduced Sn(II)O and the structural flexibility of the smaller SnO_2 NPs that resulted in correspondingly weaker binding of OH species.[49] The same group also observed that deposition of SnO_2 nanoislands onto Pt(111) resulted in enhanced electrochemical activity for the ethanol oxidation reaction (EOR).[37] This is because of strong interactions between SnO_2 and H_2O, which lead to spontaneous cleavage of O−H bonds. The authors also reported that the EOR activity strongly depended on the surface SnO_2 concentration, thereby confirming the cocatalytic effect at the oxide-metal interface.

In the remainder of this report we will show that pinhole-free, electrochemically passivating Al_2O_3 films can be deposited onto PPF electrodes. When DENs containing an average of only 55 atoms each, are deposited onto ∼15% of the Al_2O_3 surface, eT between the underlying PPF electrode and solution-phase ferrocenedimethanol ($Fc(MeOH)_2$) is recovered. This facilitated eT is insensitive to the thickness of the ALD oxide layers up to ∼3.5 nm, but partial current recovery is still observed for films up to 5.7 nm thick. Even more interestingly, DENs containing an average of 55 Pt atoms confined to Al_2O_3 thin films (PPF/Al_2O_3/G6OH(Pt_{55})), where G6OH represents sixth-generation, hydroxyl-terminated poly(amidoamine) (PAMAM) dendrimers, are electrocatalytically active for the ORR. Finally, the PPF/Al_2O_3/G6OH(Pt_{55}) constructs are robust, surviving up to at least 40 consecutive voltammetric scans and 10 min of sonication in 0.5 M H_2SO_4 without significant change in electrochemical activity.

EXPERIMENTAL SECTION

Chemicals and Materials. All chemicals were used as received. These include ferrocenedimethanol ($Fc(MeOH)_2$, 98%, Acros Organics, NY), 1-decanethiol (96%, Alfa Aesar), $HClO_4$ (+70%, ultrapure grade, J.T. Baker), and NaOH (Fischer Scientific). The following were obtained from Sigma-Aldrich: $AgNO_3$ (99%), CH_2Cl_2, $CuSO_4$, $NaBH_4$, H_2SO_4 (+98%, trace metal grade), and K_2PtCl_4. Trimethylaluminum (TMA) and O_3 gas for ALD were obtained in sealed stainless steel canisters from Sigma-Aldrich. The purge gas for ALD was high-purity N_2 gas (99.9999%, Praxair, Austin, TX).

G6OH dendrimers were purchased as a 10−25% methanol solution from Dendritech, Inc. (Midland, MI). Prior to use, the methanol was removed under vacuum. Deionized (DI) water having a resistivity of 18.2 MΩ-cm (Milli-Q gradient system, Millipore) was used for the synthesis of DENs, while all other aqueous solutions were prepared using National Exposure Research Laboratory (NERL) reagent-grade water from Thermo Scientific.

Fabrication of PPF Electrodes. PPF electrodes were fabricated using slight modifications of a procedure previously reported by our group.[14] Specifically, prior to photoresist deposition, quartz slides were cleaned sequentially in acetone, ethanol, and DI water for 10 min each. The quartz slides were further rinsed under running DI water for 1 min and then heated at 200 °C for 15 min. Next, positive-tone photoresist (AZ 1518, Capitol Scientific, Inc., Austin, TX) was spin-coated onto the slides for 10 s at 500 rpm, 45 s at 3500 rpm, and for 5 s at 500 rpm. Next, the slides were soft baked for 1 min at 100 °C and left to cool to room temperature (24 ± 1 °C). The spin coating and soft baking processes were repeated a second time to obtain lower surface roughness of the photoresist layer.

DOI: 10.1021/jacs.6b03149
J. Am. Chem. Soc. 2016, 138, 6829−6837

The photoresist-coated quartz slides were patterned by exposure to UV light through a photomask. Next, AZ 400 K developer, diluted 25% (v/v) with DI water, was used to develop the exposed photoresist. Finally, the photoresist was pyrolyzed in a quartz tube furnace under a constant flow (100 sccm) of forming gas (5% H_2 plus 95% N_2). The furnace temperature was increased from 25 to 1000 °C at 5 °C/min. The temperature was then held at 1000 °C for 1 h, and then cooled to 25 °C. The resulting PPF electrodes were stored in the laboratory ambient environment at room temperature for 14 days (more discussion about this step later) and then cut into individual electrodes using a diamond-tipped pen. The individual PPF electrodes were then rinsed under a gentle flow of reagent water, dried under a low pressure of N_2, and used within 24 h.

Prior to ALD, PPFs were plasma activated using an Oxford Instruments Plasma Lab 80+ PECVD and Etching system. Individual PPFs were exposed to the plasma (O_2, 22% and N_2, 78%) for 30 s using the following conditions: flow rate, 50 sccm; pressure, 0.03 mmHg; power, 11 W; and temperature, 50 °C. After the plasma treatment, PPFs were loaded into the ALD chamber within 10 min.

Atomic Layer Deposition. ALD was performed using a Savannah S100 Cambridge NanoTech ALD system (Ultratech, San Jose, CA). TMA was used as the Al source and O_3 as the oxygen source (neither reagent was heated). The ALD system was evacuated to <1 mmHg, and the patterned PPF substrates were heated to 150 °C for 4 min under a constant flow (20 sccm) of high-purity N_2. Next, the substrates were exposed to 10 cycles of O_3, each 15 ms long. Finally, each ALD cycle was carried out as follows: (1) a single 15 ms pulse of TMA, (2) a 20 s purge of N_2, (3) a 15 ms pulse of O_3, and (4) a 15 s purge of N_2. These four steps were repeated until the desired number of cycles had been achieved.

Surface Characterization. X-ray photoelectron spectroscopy (XPS) was carried out using a Kratos Axis Ultra spectrometer (Chestnut Ridge, NY) with an Al K_α source. Samples were grounded using Cu tape. XPS spectra were collected using a 0.10 eV step size and a band-pass energy of 80 eV. An electron flood gun was used to neutralize charge on plasma-activated PPFs and Al_2O_3-modified PPFs. Binding energies were calibrated against the C 1s line of PPF (284.4 eV).[50] CasaXPS (version 2.3.15, Casa Software, Teignmouth, UK) was used for peak fitting and analysis. A mixed Gaussian/Lorentzian model was used for symmetric line-shapes, while an asymmetric Lorentzian model was applied for asymmetric line-shapes.

Scanning electron microscope (SEM) images were collected using an EI Quanta 650 microscope and using an accelerating voltage of 15 kV.

Ellipsometric measurements were performed using a J. A. Woollam M-2000D spectroscopic ellipsometer (Lincoln, NE). Data were collected using five different angles (between 44° and 66°) for each measurement. A three-slab model was used for data analysis. The first slab was a 1.0 mm-thick layer of SiO_2 (optical constants provided by the manufacturer). The second slab was a 500 nm-thick layer of carbon (optical constants obtained experimentally using a plasma-activated PPF thin film). The third slab was Al_2O_3, and its thickness was allowed to vary. The optical constants for the Al_2O_3 layer were, however, provided by the manufacturer.

The surface roughnesses of the PPF and PPF/Al_2O_3 thin films were obtained using a Wyko NT9100 optical profilometer having a white light source and yielding 0.1 nm vertical resolution. The micro-Raman spectroscopy data were collected using a Witec Micro-Raman Alpha 300 spectrometer.

Synthesis of DENs. Pt DENs were synthesized using a previously published procedure based upon galvanic exchange.[51] Specifically, 1.0 mL of 100.0 μM sixth-generation, hydroxyl-terminated (G6OH) poly(amidoamine) (PAMAM) dendrimers was diluted in 8.68 mL of DI water. Next, 55 equiv of 20.0 mM $CuSO_4$ were pipetted into the G6OH solution. The solution was sealed and stirred under N_2 for 15 min. Next, a 5-fold molar excess of an aqueous 1.0 M $NaBH_4$ solution was added dropwise under N_2 to reduce intradendrimer Cu^{2+} to CuNPs. The reduction was carried for 45 min, and then the pH of the resulting G6OH(Cu_{55}) DENs was adjusted to 3.0 using 1.0 M $HClO_4$. Finally, sufficient aqueous 10.0 mM $PtCl_4^{2-}$ (Pt^{2+}:Cu = 1) was added dropwise (under N_2) to initiate galvanic exchange. The solution was sealed and left to stir for 60 min under N_2. One final point: the notation used to denote the DENs in this study, G6OH(Pt_{55}), is simply a representation of the Pt^{2+}:G6OH ratio used to prepare these materials. As discussed later, scanning transmission electron microscopy (STEM) results indicate a high degree of monodispersity, but of course there is still some spread in the particle-size distribution.

The Pt DENs were immobilized atop PPF/Al_2O_3 electrodes by immersing the latter in the Pt DENs solution (pH 3.0) for 30 min. After 30 min, the electrodes were rinsed under a gentle flow of NERL reagent-grade water and dried under low-pressure N_2. The newly formed PPF/Al_2O_3/G6OH(Pt_{55}) electrodes were left to dry for at least 90 min prior to use.

Characterization of Pt DENs. STEM images were obtained using a JEOL-2010F transmission electron microscope having a point-to-point resolution of 0.19 nm. 2.0 μL of the G6OH(Pt_{55}) solution was pipetted onto a lacey-carbon-over-Ni TEM grid (Electron Microscopy Sciences, Hatfield, PA). The sample was allowed to air-dry on the grid overnight prior to analysis.

UV−vis spectra of Pt DENs were collected using a Hewlett-Packard 8453 UV−vis spectrometer and 2.0 mm quartz cuvettes. The spectra were background corrected using an aqueous 10.0 μM G6OH dendrimer solution.

Electrochemical Characterization. Electrochemical measurements were obtained using a CH Instruments model CHI700D Electrochemical Analyzer (Austin, TX). The electrochemical cell was fabricated from Teflon and used a Viton O-ring to define the area of the working electrode (12.4 mm^2). For all electrochemical experiments, a $Hg/HgSO_4$ reference electrode (MSE, CH Instruments) and a Pt wire counter electrode were used. To avoid poisoning the working electrode with Hg, the reference electrode was separated from the rest of the cell by a glass frit. Cyclic voltammograms (CVs) were collected in aqueous solutions containing 1.0 mM $Fc(MeOH)_2$ as the redox-active probe, and either 0.10 M KNO_3, 0.5 M H_2SO_4, or 0.1 M $HClO_4$ as the electrolyte.

Ag electrodeposition was performed in an aqueous solution containing 0.50 mM $AgNO_3$ and 0.10 M KNO_3. The potential was stepped sufficiently negative for 50 s to reduce Ag^+ (−0.25 V vs Hg/Hg_2SO_4).

RESULTS AND DISCUSSION

Characterization of PPF Electrodes. The preparation and plasma-activation procedures used for the PPF electrodes were described in the Experimental Section, and therefore we focus here primarily on their characterization, properties, and use for electrochemical experiments.

After fabrication, the PPF electrodes were stored in the laboratory ambient for 14 days, which resulted in gradual surface oxidation, and then used for ALD within 24 h.[18,19,52] This step was included to enhance the number of active sites (C−O bonds) for Al_2O_3 nucleation. The number of C−O functionalities on the PPF surfaces was further increased by subjecting the substrates to a plasma (O_2:N_2 = 22:78) immediately prior to ALD. Through extensive optimization studies, we found that a high density of surface oxygen groups is critical to the formation of ultrathin, pinhole-free Al_2O_3 ALD layers.

XPS analysis was used to confirm oxygenation of the PPF electrode surfaces (Supporting Information, Figure S1). The results show that immediately after fabrication the O 1s and C 1s peaks are present at 532 and 284.4 eV, respectively. After 14 days in the laboratory atmosphere, the amount of surface O increases ∼1.7 times. Following 30 s of O_2/N_2 plasma treatment, the surface oxygen signal increases by another factor of 2. The additional oxygenated functionalities are observed at 286.2 and 288.6 eV, and we assign these peaks to phenolic and carboxylic carbon, respectively.[53−55]

DOI: 10.1021/jacs.6b03149
J. Am. Chem. Soc. 2016, 138, 6829−6837

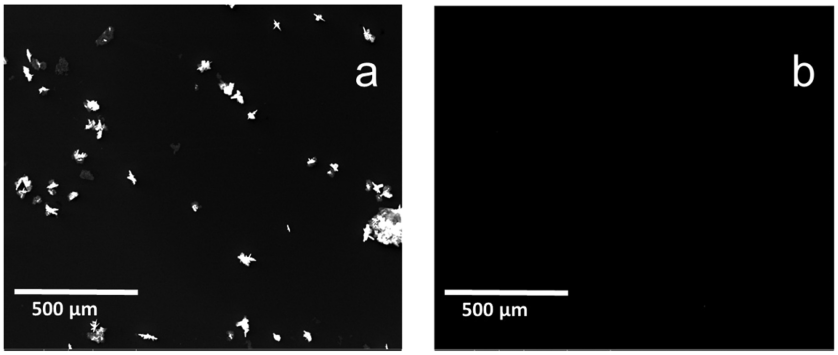

Figure 1. SEM micrographs of Ag electrodeposited onto PPF/Al_2O_3(30) electrodes (a) without and (b) with plasma preactivation of the carbon surface for 30 s. The Ag was electrodeposited by holding the potential at −0.25 V (vs an Hg/Hg_2SO_4 reference electrode) for 50 s in a solution containing 0.50 mM $AgNO_3$ and 0.10 M KNO_3.

The PPFs were also characterized using optical profilometry. At the lateral and vertical resolutions of the instrument (0.1 μm and 0.1 nm, respectively), the data reveal smooth, uniform surfaces that are free of cracks. The root-mean-square (rms) roughness, averaged over an area of 48 μm × 64 μm for eight different PPF electrodes was ∼0.64 nm (Figure S2). This value is comparable to rms roughness values reported in the literature, which range from 0.2 and 0.7 nm, but these values were measured over much smaller areas (e.g., 0.5 μm × 0.5 μm).[56−58]

Finally, micro-Raman spectroscopy was used to study the near-surface structure of the PPFs (Figure S3). The analysis revealed two Raman-active peaks.[58] A peak at 1600 cm^{-1} arises from the E_{2g} mode at the Γ-point commonly observed for glassy carbon and other sp^2 carbon systems.[59,60] The A_{1g} peak at ∼1360 cm^{-1} is associated with loss of symmetry at the boundaries of graphite sheets.[58] Taken together, these results suggest that the PPF electrodes are uniform and structurally similar to glassy carbon.[60]

Properties and Stability of Al_2O_3 ALD Films. The procedure used to prepare the Al_2O_3 ALD films is provided in the Experimental Section. For the purposes of our experiments, their critical characteristics are that they have well-defined thicknesses, that they be uniform over macroscopic dimensions, and that they be pinhole free.

The thicknesses of the Al_2O_3 films were measured using spectroscopic ellipsometry. The data revealed linear growth of the Al_2O_3 films with a growth rate of 0.086 ± 0.005 nm/cycle (Figure S4). This value is consistent with the growth rate provided by the ALD system manufacturer for the deposition of Al_2O_3 onto Si(100) at 150 °C (0.087 nm/cycle).[61]

Optical profilometry revealed that the Al_2O_3 films are uniform and free of cracks. The value for the average rms roughness, determined using eight independently prepared PPF electrodes coated with 2.5 nm-thick Al_2O_3 films, was ∼0.60 nm over an area of 48 μm × 64 μm (Figure S5). This value is almost the same as the corresponding rms value for the underlying PPF electrodes prior to ALD (∼0.64 nm) discussed in the previous section.

Defects in the Al_2O_3 films were visualized by combining electrodeposition and SEM.[62] This analysis was carried out as follows. First, Al_2O_3-modified PPF electrodes were immersed in a solution containing 0.50 mM $AgNO_3$ and 0.10 M KNO_3, and then the potential was stepped to −0.25 V for 50 s.[14] Under these conditions, Ag electrodeposits into pinholes that might be present in the ALD film. Even subnanometer defects are revealed using this approach, because the presence of the pinhole, though smaller than the resolution of SEM, is magnified by the electrodeposited Ag islands. It is important to point out, however, that while this method is useful for approximating the number and location of defects in ALD films, it does not reflect their true size.[14]

Figure 1 shows the result of this experiment. Figure 1a is an SEM micrograph obtained after Ag electrodeposition onto a PPF electrode coated with 30 ALD cycles of Al_2O_3 (henceforth, PPF/Al_2O_3(30)), but without the 30 s plasma treatment prior to ALD. In contrast, when the exact same fabrication steps are used to prepare the Al_2O_3 film, except using a 30 s plasma pretreatment prior to ALD, pinhole-free films result over macroscopic lateral dimensions (e.g., 1.0 cm × 1.2 cm, Figure 1b). Clearly, the plasma-induced oxygenation of the PPF surface is critical for the formation of ultrathin, pinhole-free electrodes.

The ALD films used in this study are stable in the relevant electrochemical environments. For example, Figure 2a shows the first and fortieth cyclic voltammograms (CVs) obtained using a solution containing 1.0 mM $Fc(MeOH)_2$ plus 0.1 M KNO_3 and a PPF/Al_20_3(30) electrode. These data were recorded at neutral pH, but the stability of Al_2O_3 under acidic conditions is also crucial, because, as discussed later, immobilization of G6OH(Pt_{55}) DENs is carried out at pH 3.0. To test the stability of the films in acid, a PPF/Al_20_3(30) electrode was immersed in a pH 3.0 $HClO_4$ solution for 30 min. Figure 2b shows CVs of $Fc(MeOH)_2$ before and after this acid treatment. Clearly changes to the ALD film are minimal under the conditions required for Pt DEN immobilization.

Immobilization and Characterization of Pt DENs atop Al_2O_3-Modified PPF Electrodes. Prior to immobilization atop Al_2O_3-modified PPF electrodes, the free G6OH(Pt_{55}) DENs were characterized using UV−vis spectroscopy and STEM (Figures S6 and S7, respectively). The results are fully consistent with prior reports,[51,63] and they indicate the presence of Pt_{55} DENs having a size of 1.3 ± 0.2 nm.

The procedure for preparing the PPF/Al_2O_3/G6OH(Pt_{55}) layered structure was discussed in the Experimental Section. To confirm the presence of both the dendrimers and Pt on the Al_2O_3 surface, we carried out XPS measurements (Figure 3a). The N(1s) peak at 400.4 eV confirms the presence of the PAMAM dendrimers, while the Pt(4d3/2), Pt(4d5/2), Pt(4f) and Pt(4p) peaks at 332.1 eV, 315.4 eV, ∼72.2 and 519.4 eV, respectively, confirm the presence of Pt. The location of the Pt(4f) peak at a little higher binding energy than that of bulk Pt

DOI: 10.1021/jacs.6b03149
J. Am. Chem. Soc. 2016, 138, 6829−6837

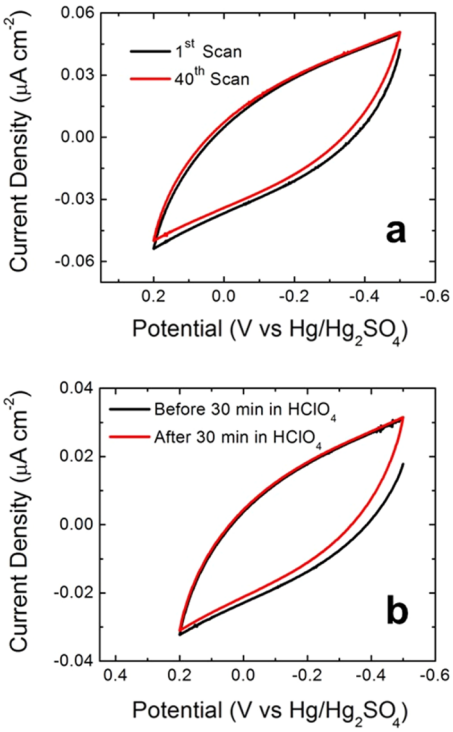

Figure 2. (a) First (black) and 40th (red) CVs for a PPF/Al_2O_3(30) electrode. (b) CVs for a PPF/Al_2O_3(30) electrode before (black) and after (red) a 30 min exposure of the electrode to a pH 3.0 $HClO_4$ solution. The CVs were obtained in an aqueous solutions containing 1.0 mM $Fc(MeOH)_2$ and 0.10 M KNO_3. The scan rate was 10 mV s^{-1}.

(71.1 eV)[50] is consistent with previously reported XPS measurements for Pt DENs and is likely a consequence of their small size and the presence of the dendrimers.[51] The Al (2p) peak is also observed, indicating that Al_2O_3 is still present on the surface after immobilization of the Pt DENs.

The presence of Pt on the electrode surface was also confirmed electrochemically by obtaining CVs of a PPF/Al_2O_3(30)/G6OH(Pt_{55}) electrode in a 0.1 M aqueous $HClO_4$ solution. Figure 3b shows both the first and the fortieth CVs. The nearly identical appearance of these two scans demonstrates the stability of the DENs on the Al_2O_3 surface. In both scans, the Pt oxidation region is observed starting at ~0.2 V, and the corresponding oxide reduction peak is at ~0.07 V. The characteristic hydride peaks at potentials < −0.4 V are also present. All of these characteristics are consistent with previous reports for G6OH(Pt_{55}) DENs immobilized directly on carbon electrodes.[5,11,64,51] Integration of the hydride oxidation peaks, coupled with a calculation we have used previously to determine DEN coverage,[65,66] indicate that ~15% of the Al_2O_3 surface is covered by DENs.

To further demonstrate the structural stability of PPF/Al_2O_3(30)/G6OH(Pt_{55}) electrodes, CVs of $Fc(MeOH)_2$ were obtained before and after sonication in 0.5 M H_2SO_4 for 10 min. The results (Figure 3c) indicate very little change arising from this accelerated form of stability testing. On the basis of the data shown in Figure 3, we conclude that the interaction between the dendrimer host and the Al_2O_3 surface is quite robust.

Pt DEN-Mediated eT. Through extensive testing, we found that Al_2O_3 films thicker than 2.5 nm (30 ALD cycles) are necessary to completely passivate eT between the underlying PPF electrode and solution-phase $Fc(MeOH)_2$. For example,

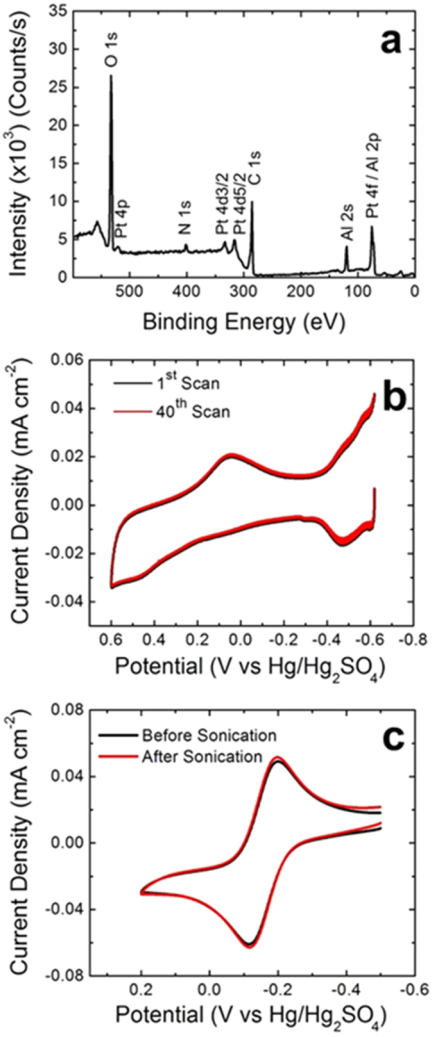

Figure 3. (a) XPS spectrum of a PPF/Al_2O_3(30)/G6OH(Pt_{55}) electrode. (b) CVs of the first (black) and fortieth (red) scans of a PPF/Al_2O_3(30)/G6OH(Pt_{55}) electrode in an Ar-purged aqueous 0.1 M $HClO_4$ solution. The scan started at −0.62 V and proceeded initially in the positive direction. The scan rate was 100 mV/s. (c) CVs of a PPF/Al_2O_3(30)/G6OH(Pt_{55}) electrode before (black) and after (red) sonication in an aqueous 0.5 M H_2SO_4 solution for 10 min. These CVs were obtained in an aqueous solutions containing 1.0 mM $Fc(MeOH)_2$ and 0.10 M KNO_3. The scan rate was 10 mV s^{-1}.

Figure 4a compares the CV response of a bare PPF electrode and a PPF/Al_2O_3(30) electrode. The inset in Figure 4a, which shows the potential region around E° for $Fc(MeOH)_2$, clearly indicates complete electrode passivation. These results can be compared to the CVs shown in Figure 4b, which compare a PPF/Al_2O_3(30)/G6OH(Pt_{55}) electrode with that of a PPF/Al_2O_3(30)/G6OH (no Pt_{55} DENs) electrode. The obvious result is that electroactivity is completely reactivated in the presence of Pt DENs. Indeed, the shape of two black CVs in Figure 4 are nearly identical. These results demonstrate that the observed current recovery of $Fc(MeOH)_2$ is facilitated solely by the Pt DENs and that it is not influenced by the PAMAM dendrimer host, the electrolyte solution, or electrochemical cycling.

Location of Pt DENs. We have previously shown that Pt DENs prepared by galvanic exchange are confined within their dendrimer hosts.[63,64] It is important, however, to demonstrate that they remain confined following immobilization onto the

DOI: 10.1021/jacs.6b03149
J. Am. Chem. Soc. 2016, 138, 6829−6837

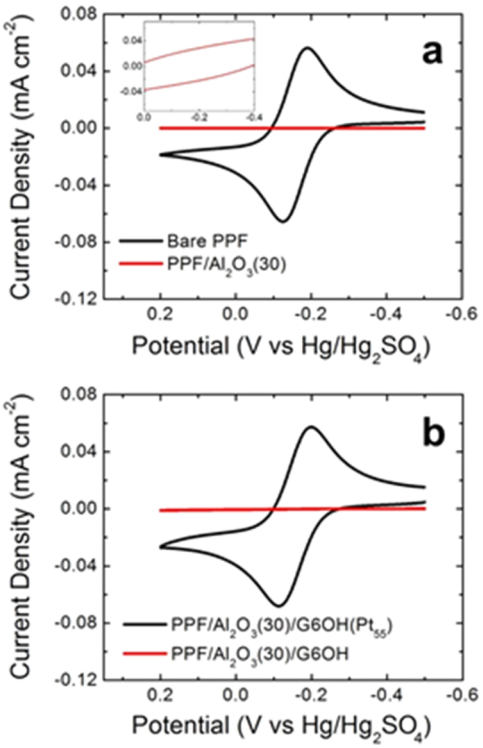

Figure 4. (a) CVs obtained at a bare PPF electrode (black) and a PPF/Al_2O_3(30) electrode (red). The inset is an expanded view of the potential region around E° for $Fc(MeOH)_2$. (b) CVs obtained at a PPF/Al_2O_3(30)/G6OH electrode (red) and a PPF/Al_2O_3(30)/G6OH(Pt_{55}) electrode (black). The solutions contained aqueous 1.0 mM $Fc(MeOH)_2$ and 0.10 M KNO_3. The scan rate was 10 mV s^{-1}.

Al_2O_3 surfaces used in this study. In other words, that the presence of Al_2O_3 does not somehow extract the Pt DENs. This point was addressed by performing a Pt DENs poisoning experiment that we have reported previously.[64]

The poisoning experiment was carried out as follows. First, a PPF/Al_2O_3(30)/G6OH(Pt_{55}) electrode was immersed in ethanol. Second, sufficient 1-decanethiol was added to make the solution 3.0 mM in ethanol. Third, after 20 min, the electrode was rinsed in ethanol and NERL reagent-grade water. Finally, a CV was obtained in an aqueous solution containing 1.0 mM $Fc(MeOH)_2$ and 0.1 M KNO_3. The resulting low current (red CV in Figure 5) indicates that the Pt DENs are nearly fully passivated by surface-confined 1-decanethiol. In contrast, when the same experiment is carried out using a CH_2Cl_2 in place of ethanol the black CV obtains.

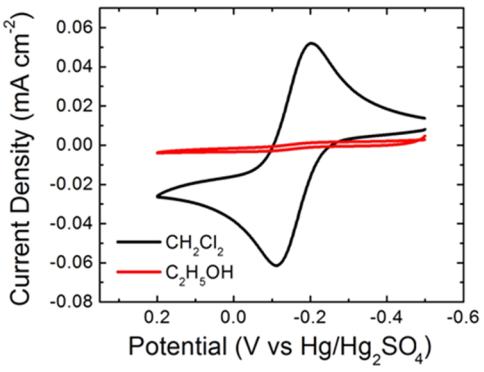

Figure 5. CVs obtained after exposure of PPF/Al_2O_3(30)/G6OH-(Pt_{55}) electrodes to 1-decanethiol in either CH_2Cl_2 (black) or ethanol (red) for 20 min. The aqueous electrolyte solution contained 1.0 mM $Fc(MeOH)_2$ and 0.10 M KNO_3. The scan rate was 10 mV s^{-1}.

We interpret these results as follows. Ethanol is a good solvent for PAMAM dendrimers, and therefore their branches are solvated allowing 1-decanethiol to pass to the surface of the encapsulated Pt DENs. This in turn passivates the surface of the DENs with 1-decanethiol and so little faradaic current due to $Fc(MeOH)_2$ is observed. In contrast, CH_2Cl_2 is a very poor solvent for PAMAM dendrimers, and therefore their branches collapse onto the surface of the Pt DENs rendering them inaccessible to the thiol and hence unpoisoned. Accordingly, when the electrode is rinsed and placed back in the electrolyte solution, the original (unhindered) voltammetry is observed (black CV in Figure 5). If the DENs were not confined within the dendrimers, both CVs (not just the red one) in Figure 5 would exhibit little current. Accordingly, these results confirm that the Pt DENs are present within the dendrimers and that current recovery on the Al_2O_3 surface is mediated by PtNPs encapsulated within the dendrimers and not by bare PtNPs.

Effect of Al_2O_3 Thickness on Pt DEN-Mediated eT. Figure 6a presents CVs obtained using PPF/Al_2O_3(n)/G6OH(Pt_{55}) electrodes, where n represents the number of ALD cycles used to prepare the Al_2O_3 layer. As discussed in the context of Figure 4, the CV of $Fc(MeOH)_2$ corresponding to the PPF/Al_2O_3(30)/G6OH(Pt_{55}) electrode is nearly identical

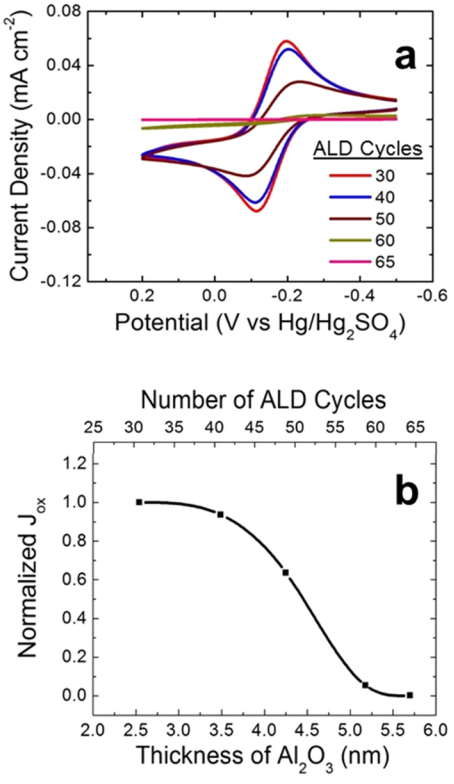

Figure 6. (a) CVs of PPF/Al_2O_3(n)/G6OH(Pt_{55}) electrodes (n is the number of ALD cycles, as indicated in the legend). The aqueous electrolyte solution contained 1.0 mM $Fc(MeOH)_2$ and 0.10 M KNO_3. The scan rate was 10 mV s^{-1}. (b) Normalized maximum current density (J_{ox}), obtained from the CVs in (a), as a function of the number of ALD cycles and the thickness of the Al_2O_3 ALD layers on the PPF electrodes. The value of J_{ox} for a bare PPF electrode was used to normalize the currents.

DOI: 10.1021/jacs.6b03149
J. Am. Chem. Soc. 2016, 138, 6829−6837

to that obtained using a bare PPF electrode. As the number of ALD cycles increase from 30 to 65, however, the faradaic current decreases slowly at first and proceeds to full passivation at n = 65.

The plot shown in Figure 6b is a quantitative representation of the normalized current density (J_{ox}), obtained from the peaks of the $Fc(MeOH)_2$ oxidation waves shown in Figure 6a, as a function of the Al_2O_3 thickness and number of ALD cycles. This plot, along with the observation of an increase in splitting between the oxidation and reduction waves as n increases, suggests that a small but detectable decrease in eT rate occurs for an Al_2O_3 thickness of 3.5 nm (40 ALD cycles). Much larger decreases are observed for thicknesses ≥4.3 nm (≥50 ALD cycles). In other words, for thicknesses of Al_2O_3 < 3.5 nm, eT between $Fc(MeOH)_2$ and the $G6OH(Pt_{55})$ DENs is the rate limiting step.[31,32,44] For thicknesses >3.5 nm the eT kinetics change from thickness independent to thickness dependent, suggesting that eT from the PPF electrode to $G6OH(Pt_{55})$ DENs becomes the limiting source of charge transfer.

As discussed in the introduction, Chazalviel and Allongue reported a theoretical framework for understanding the distance dependence of eT across metal/insulator/metal-NP systems.[44] This model suggests that 55-atom DENs, which are have a diameter of ∼1.3 nm, should exhibit distance independent eT up to insulator thicknesses of ∼1.6 nm. The distance we observe for this transition is ∼3.5 nm. At present we do not understand the origin of this discrepancy.

It is possible to extract the effective standard heterogeneous eT rate constant from the brown-colored CV shown in Figure 6a, which corresponds to the $PPF/Al_2O_3(50)/G6OH(Pt_{55})$ construct, using the Nicholson and Shain model[67] and a value for the diffusion coefficient of oxidized $Fc(MeOH)_2$ of 6.7×10^{-6} cm^2/s.[68,69] The Al_2O_3 layer in this film is 4.3 nm thick, and we estimate the standard eT rate constant to be 1.43×10^{-3} cm/s. This value is just a little higher than previously reported values for NP-reactivated eT across organic layers having thicknesses close to 4.3 nm.[26,30,31,70,71]

The Oxygen Reduction Reaction (ORR) at a Reactivated Al_2O_3 Thin Film Electrode. Our long-term interest is in developing a better understanding of electrocatalytic reactions in which an oxide surface participates. As a first step toward that goal, we examined the voltammetry of three different types of electrodes in a 0.1 M $HClO_4$ solution saturated with O_2 (Figure 7).

Over the potential range examined (±0.40 V), the bare PPF electrode is catalytically inactive for the ORR. Likewise, a $PPF/Al_2O_3(30)$ electrode is also inactive. In contrast, the $PPF/Al_2O_3(30)/G6OH(Pt_{55})$ is highly active. In fact, although the peak current density of $PPF/Al_2O_3(30)/G6OH(Pt_{55})$ electrode is higher compared to a bulk Pt electrode, their onset potentials are nearly the same (Figure 7, inset). A control experiment was also carried out in which a $PPF/Al_2O_3(30)/G6OH(Pt_{55})$ electrode was scanned in an O_2-free 0.1 M $HClO_4$ solution. The result displayed only a small background current (Figure S8), confirming that the peak shown in Figure 7 corresponds to the ORR.

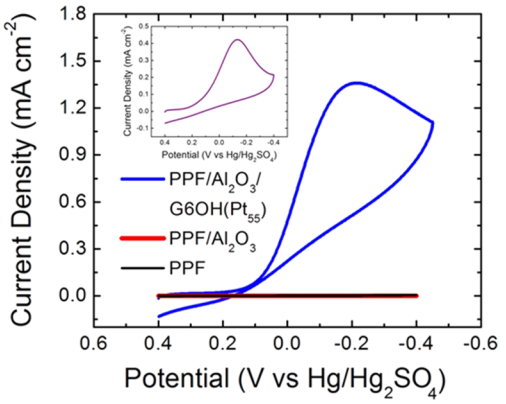

Figure 7. CVs obtained in an aqueous O_2-saturated 0.1 M $HClO_4$ solution at a bare PPF electrode (black), a $PPF/Al_2O_3(30)$ electrode (red), and a $PPF/Al_2O_3(30)/G6OH(Pt_{55})$ electrode (blue). For comparison, the inset is a CV obtained at a macroscopic Pt electrode. The scan rate was 50 mV/s in all cases.

SUMMARY AND CONCLUSIONS

Here we have shown that eT between a PPF electrode and $Fc(MeOH)_2$ can be completely passivated by Al_2O_3 films as thin as 2.5 nm if the PPF electrode is plasma-activated before ALD. One of the key findings is that deposition of 1.3 nm $G6OH(Pt_{55})$ DENs atop these insulating films leads to complete recovery of faradaic eT. Most importantly, however, the $PPF/Al_2O_3/G6OH(Pt_{55})$ electrodes are stable and active for electrocatalytic reactions, in this case the ORR.

The $PPF/Al_2O_3/G6OH(Pt_{55})$ system is unique, because it permits the study of electrocatalytic reactions in the presence and absence of NP/support interactions. That is, the DENs in this model system are not in a direct contact with the Al_2O_3 support. Therefore, support effects do not manifest themselves when DENs are used for studying electrocatalytic reactions. If, however, the dendrimers can be cleanly removed without passivating or aggregating the encapsulated PtNPs, then it will be possible to directly examine the effect of the PtNP/oxide-support interaction on electrocatalytic reactions. Ongoing studies suggest that it is indeed possible to remove the dendrimer, and the results of these experiments, as well as the outcome of more complex electrocatalytic reactions, will be reported in due course.

ASSOCIATED CONTENT

Supporting Information

The Supporting Information is available free of charge on the ACS Publications website at DOI: 10.1021/jacs.6b03149.

XPS of a PPF electrode and a plasma-activated PPF electrodes, optical profilometry of a plasma-activated PPF electrode, Raman spectrum of a PPF electrode, ellipsometric thickness measurements of Al_2O_3 films as a function of the number of ALD cycles, optical profilometry of an $Al_2O_3(30)$ film deposited atop a plasma-activated PPF electrode, UV−vis spectra of $G6OH(Pt_{55})$ DENs and their precursors, STEM of $G6OH(Pt_{55})$ DENs, and CVs of $PPF/Al_2O_3(30)/G6OH(Pt_{55})$ electrodes in 0.1 M $HClO_4$ solutions purged with O_2 or Ar. (PDF)

AUTHOR INFORMATION

Corresponding Author

*crooks@cm.utexas.edu

Notes

The authors declare no competing financial interest.

DOI: 10.1021/jacs.6b03149
J. Am. Chem. Soc. 2016, 138, 6829−6837

■ ACKNOWLEDGMENTS

We gratefully acknowledge support from the Chemical Sciences, Geosciences, and Biosciences Division, Office of Basic Energy Sciences, Office of Science, U.S. Department of Energy (Contract: DE-FG02-13ER16428). We thank the Robert A. Welch Foundation (Grant F-0032) for sustained support of our research. We also thank Dr. Long Luo and Zhiyao Duan for helpful discussions.

■ REFERENCES

(1) Anderson, R. M.; Yancey, D. F.; Zhang, L.; Chill, S. T.; Henkelman, G.; Crooks, R. M. *Acc. Chem. Res.* **2015**, *48*, 1351−1357.
(2) Peng, X.; Pan, Q.; Rempel, G. L. *Chem. Soc. Rev.* **2008**, *37*, 1619.
(3) Bronstein, L. M.; Shifrina, Z. B. *Chem. Rev.* **2011**, *111*, 5301−5344.
(4) Lang, H.; May, R. A.; Iversen, B. L.; Chandler, B. D. *J. Am. Chem. Soc.* **2003**, *125*, 14832−14836.
(5) Myers, V. S.; Weir, M. G.; Carino, E. V.; Yancey, D. F.; Pande, S.; Crooks, R. M. *Chem. Sci.* **2011**, *2*, 1632.
(6) Astruc, D. *Nanoparticles and Catalysis*; Wiley-VCH: Weinheim, 2008; pp 1−33.
(7) Aikens, C. M. *J. Phys. Chem. Lett.* **2011**, *2*, 99−104.
(8) Cuenya, B. R. *Thin Solid Films* **2010**, *518*, 3127−3150.
(9) Zhang, L.; Anderson, R. M.; Crooks, R. M.; Henkelman, G. *Surf. Sci.* **2015**, *640*, 65−72.
(10) Zhang, L.; Iyyamperumal, R.; Yancey, D. F.; Crooks, R. M.; Henkelman, G. *ACS Nano* **2013**, *7*, 9168−9172.
(11) Anderson, R. M.; Zhang, L.; Loussaert, J. A.; Frenkel, A. I.; Henkelman, G.; Crooks, R. M. *ACS Nano* **2013**, *7*, 9345−9353.
(12) Luo, L.; Zhang, L.; Henkelman, G.; Crooks, R. M. *J. Phys. Chem. Lett.* **2015**, *6*, 2562−2568.
(13) Pozun, Z. D.; Rodenbusch, S. E.; Keller, E.; Tran, K.; Tang, W.; Stevenson, K. J.; Henkelman, G. *J. Phys. Chem. C* **2013**, *117*, 7598−7604.
(14) Loussaert, J. A.; Fosdick, S. E.; Crooks, R. M. *Langmuir* **2014**, *30*, 13707−13715.
(15) Kim, H. J.; Kearney, K. L.; Le, L. H.; Pekarek, R. T.; Rose, M. J. *ACS Appl. Mater. Interfaces* **2015**, *7*, 8572−8584.
(16) Hoex, B.; Schmidt, J.; Bock, R.; Altermatt, P. P.; van de Sanden, M. C. M.; Kessels, W. M. M. *Appl. Phys. Lett.* **2007**, *91*, 112107.
(17) Liu, Z. H.; Ng, G. I.; Zhou, H.; Arulkumaran, S.; Maung, Y. K. T. *Appl. Phys. Lett.* **2011**, *98*, 113506.
(18) Ranganathan, S.; Mccreery, R.; Majji, S. M.; Madou, M. *J. Electrochem. Soc.* **2000**, *147*, 277−282.
(19) Ranganathan, S.; McCreery, R. L. *Anal. Chem.* **2001**, *73*, 893−900.
(20) Grabar, K. C.; Allison, K. J.; Baker, B. E.; Bright, R. M.; Brown, K. R.; Freeman, R. G.; Fox, A. P.; Keating, C. D.; Musick, M. D.; Natan, M. J. *Langmuir* **1996**, *12*, 2353−2361.
(21) Freeman, G. R.; Grabar, K. C.; Allison, K. J.; Bright, R. M.; Davis, J. A.; Guthrie, A. P.; Hommer, M. B.; Jackson, M. A.; Smith, P. C.; Walter, D. G.; et al. *Science* **1995**, *267*, 1629.
(22) Bethell, D.; Brust, M.; Schiffrin, D. J.; Kiely, C. *J. Electroanal. Chem.* **1996**, *409*, 137−143.
(23) Brust, M.; Bethell, D.; Kiely, C. J.; Schiffiin, D. J. *Langmuir* **1998**, *14*, 5425−5429.
(24) Horswell, S. L.; O'Nei, I. A.; Schiffrin, D. J. *J. Phys. Chem. B* **2003**, *107*, 4844−4854.
(25) Zhao, J.; Bradbury, C. R.; Fermin, D. J. *J. Phys. Chem. C* **2008**, *112*, 6832−6841.
(26) Kissling, G. P.; Miles, D. O.; Fermín, D. J. *Phys. Chem. Chem. Phys.* **2011**, *13*, 21175.
(27) Zhao, J.; Bradbury, C. R.; Huclova, S.; Potapova, I.; Carrara, M.; Fermín, D. J. *J. Phys. Chem. B* **2005**, *109*, 22985−22994.
(28) Bradbury, C. R.; Zhao, J.; Fermín, D. J. *J. Phys. Chem. C* **2008**, *112*, 10153−10160.
(29) Zhao, J.; Wasem, M.; Bradbury, C. R.; Fermín, D. J. *J. Phys. Chem. C* **2008**, *112*, 7284−7289.
(30) Shein, J. B.; Lai, L. M. H.; Eggers, P. K.; Paddon-Row, M. N.; Gooding, J. J. *Langmuir* **2009**, *25*, 11121−11128.
(31) Barfidokht, A.; Ciampi, S.; Luais, E.; Darwish, N.; Gooding, J. J. *Anal. Chem.* **2013**, *85*, 1073−1080.
(32) Gooding, J. J.; Alam, M. T.; Barfidokht, A.; Carter, L. *J. Braz. Chem. Soc.* **2013**, *35*, 418−426.
(33) Nuzzo, R. G.; Allara, D. L. *J. Am. Chem. Soc.* **1983**, *105*, 4481−4483.
(34) Kim, J.; Kim, B.-K.; Cho, S. K.; Bard, A. J. *J. Am. Chem. Soc.* **2014**, *136*, 8173−8176.
(35) Sasaki, K.; Zhang, L.; Adzic, R. R. *Phys. Chem. Chem. Phys.* **2008**, *10*, 159−167.
(36) Zhang, J.; Vukmirovic, M. B.; Sasaki, K.; Nilekar, A. U.; Mavrikakis, M.; Adzic, R. R. *J. Am. Chem. Soc.* **2005**, *127*, 12480−12481.
(37) Zhou, W.-P.; Axnanda, S.; White, M. G.; Adzic, R. R.; Hrbek, J. *J. Phys. Chem. C* **2011**, *115*, 16467−16473.
(38) Wu, Z.-S.; Zhou, G.; Yin, L.-C.; Ren, W.; Li, F.; Cheng, H.-M. *Nano Energy* **2012**, *1*, 107−131.
(39) Wang, D.; Kou, R.; Choi, D.; Yang, Z.; Nie, Z.; Li, J.; Saraf, L. V.; Hu, D.; Zhang, J.; Graff, G. L.; et al. *ACS Nano* **2010**, *4*, 1587−1595.
(40) Robel, I.; Bunker, B. A.; Kamat, P. V. *Adv. Mater.* **2005**, *17*, 2458−2463.
(41) Diao, P.; Liu, Z. *J. Phys. Chem. B* **2005**, *109*, 20906−20913.
(42) Su, L.; Gao, F.; Mao, L. *Anal. Chem.* **2006**, *78*, 2651−2657.
(43) Ye, M.; Gong, J.; Lai, Y.; Lin, C.; Lin, Z. *J. Am. Chem. Soc.* **2012**, *134*, 15720−15723.
(44) Chazalviel, J.-N.; Allongue, P. *J. Am. Chem. Soc.* **2011**, *133*, 762−764.
(45) Chai, H.; Liu, H.; Guo, X.; Zheng, D.; Kutes, Y.; Huey, B. D.; Rusling, J. F.; Hu, N. *Electroanalysis* **2012**, *24*, 1129−1140.
(46) Baturina, O. A.; Garsany, Y.; Zega, T. J.; Stroud, R. M.; Schull, T.; Swider-Lyons, K. E. *J. Electrochem. Soc.* **2008**, *155*, B1314.
(47) Garsany, Y.; Epshteyn, A.; Purdy, A. P.; More, K. L.; Swider-Lyons, K. E. *J. Phys. Chem. Lett.* **2010**, *1*, 1977−1981.
(48) Korovina, A.; Garany, Y.; Epshteyn, A.; Purdy, A. P.; More, K.; Swider-Lyons, K. E.; Ramaker, D. E. *J. Phys. Chem. C* **2012**, *116*, 18175−18183.
(49) Zhou, W.-P.; An, W.; Su, D.; Palomino, R.; Liu, P.; White, M. G.; Adzic, R. R. *J. Phys. Chem. Lett.* **2012**, *3*, 3286−3290.
(50) *Nist X-Ray Photoelectron Spectroscopy Database*, Version 4.1; National Institute of Standards and Technology: Gaithersburg, MD, 2012; http://srdata.nist.gov/xps/.
(51) Pande, S.; Weir, M. G.; Zaccheo, B. A.; Crooks, R. M. *New J. Chem.* **2011**, *35*, 2054.
(52) Donner, S.; Li, H.-W.; Yeung, E. S.; Porter, M. D. *Anal. Chem.* **2006**, *78*, 2816−2822.
(53) Jones, C.; Sammann, E. *Carbon* **1990**, *28*, 515−519.
(54) Cabaniss, G. E.; Diamantis, A. A.; Murphy, W. R.; Linton, R. W.; Meyer, T. J. *J. Am. Chem. Soc.* **1985**, *107*, 1845−1853.
(55) Moulder, J. F.; Stickle, W. F.; Sobol, P. E.; Bomben, K. D. *Handbook of X-ray Photoelectron Spectroscopy*; Physical Electronics USA, Inc.: Chanhassen, MN, 1995.
(56) Yu, S. S. C.; Downard, A. J. *Langmuir* **2007**, *23*, 4662−4668.
(57) Anariba, F.; DuVall, S. H.; McCreery, R. L. *Anal. Chem.* **2003**, *75*, 3837−3844.
(58) Kostecki, R.; Schnyder, B.; Alliata, D.; Song, X.; Kinoshita, K.; Kotz, R. *Thin Solid Films* **2001**, *396*, 36−43.
(59) Childres, I.; Jauregui, L. A.; Park, W.; Cao, H.; Chen, Y. P. *Dev. Photon Mater. Res.* **2013**, 978−981.
(60) Nathan, M. I.; Smith, J. E.; Tu, K. N. *J. Appl. Phys.* **1974**, *45*, 2370.
(61) Cambridge NanoTech, Simply ALD. www.cambridgenanotech.com (accessed Feb 5, 2015).
(62) Sun, L.; Crooks, R. M. *J. Electrochem. Soc.* **1991**, *138*, L23−L25.
(63) Anderson, R. M.; Yancey, D. F.; Loussaert, J. A.; Crooks, R. M. *Langmuir* **2014**, *30*, 15009−15015.
(64) Ye, H.; Crooks, R. M. *J. Am. Chem. Soc.* **2005**, *127*, 4930−4934.

DOI: 10.1021/jacs.6b03149
J. Am. Chem. Soc. 2016, 138, 6829−6837

(65) Ye, H.; Crooks, J. A.; Crooks, R. M. *Langmuir* **2007**, *23*, 11901−11906.
(66) Dumitrescu, I.; Yancey, D. F.; Crooks, R. M. *Lab Chip* **2012**, *12*, 986.
(67) Bard, A. J.; Faulkner, L. R. *Electrochemical Methods: Fundamentals and Applications*, 2nd ed.; Wiley: New York, 2001; pp 242−243.
(68) Anicet, N.; Bourdillon, C.; Moiroux, J.; Savéant, J.-M. *J. Phys. Chem. B* **1998**, *102*, 9844−9849.
(69) Mampallil, D.; Mathwig, K.; Kang, S.; Lemay, S. G. *J. Phys. Chem. Lett.* **2014**, *5*, 636−640.
(70) Dyne, J.; Lin, Y.-S.; Lai, L. M. H.; Ginges, J. Z.; Luais, E.; Peterson, J. R.; Goon, I. Y.; Amal, R.; Gooding, J. J. *ChemPhysChem* **2010**, *11*, 2807−2813.
(71) Sun, P.; Mirkin, M. V. *Anal. Chem.* **2006**, *78*, 6526−6534.

DOI: 10.1021/jacs.6b03149
J. Am. Chem. Soc. 2016, 138, 6829−6837